Verification and Validation of Computational Fluid Dynamics Simulations of Compound Channel Flow

M. S. Filonovich[1,2] , R. Azevedo[1] , L. R. Rojas-Solorzano[3] and J. B. Leal[1,2]

[1]Departamento de Engenharia Civil
Faculdade de Ciências e Tecnologia/Universidade Nova de Lisboa
Campus de Caparica, Caparica 2829-516
PORTUGAL
[2]CEHIDRO, Instituto Superior Técnico
Av. Rovisco Pais, Lisboa 1049-001
PORTUGAL
[3]Universidad Simón Bolívar, Caracas
VENEZUELA
E-mail: m.filonovich@fct.unl.pt

Abstract: *In this study the verification and validation of a 2nd order turbulence closure model is performed for an experimental compound channel flow, where the velocity field was measured by a Laser Doppler Velocimeter. Detailed Explicit Algebraic Reynolds Stress Model (EARSM) simulation is reported. The Grid Convergence Index (GCI) approach proposed by Roache (1998) was adopted to evaluate the uncertainty associated to grid resolution. The velocity components, the turbulent kinetic energy (TKE) and the dissipation rate were used as variables of interest. The GCI results present low values for the streamwise velocity, TKE and dissipation rate, but higher values in what concerns vertical and spanwise velocities. This indicates that the mean primary flow has converged but the secondary flow field still depends on grid resolution. Based on GCI values distribution, the mesh was locally refined. Comparison of numerical and experimental results shows good agreement.*

Keywords: *CFD, GCI, EARSM, compound channel, verification, validation.*

1. INTRODUCTION

During the last few decades there has been a big increase in computer simulations of practical fluid dynamics problems. There are many Computational Fluid Dynamics (CFD) codes, commercial and in-house, that simulate the behavior of turbulent flows. However, nowadays in CFD simulations it is no longer enough just to produce a solution, but also a credibility analysis of the numerical model should be performed (*e.g.* Celik, 2008). This analysis consists of two fundamental steps: verification and validation.

Verification is principally a mathematics and computer science issue (Roache, 1998) which consists of two steps: i) code verification, its assessment consists of accumulating evidence certifying that the code does not have algorithmic or programming errors; ii) solution verification, based on the accumulation of evidence that a specific calculation is correct and accurate, and requires confirmation of grid convergence (Oberkampf, 2002).

Validation is primarily a physical sciences issue (Roache, 1998), which shows the assessment of the accuracy of a computational model by comparison with experimental data. In other words, according to Roache (1997) verification is “solving the equations right” and validation is “solving the right equations”.

Several authors have contributed to the verification of CFD solutions (among others, Celik, 2008, Hardy *et al*., 2003, Roache, 1997), some have contributed to highly accurate numerical solutions while others have contributed to analytical solutions useful for verification. In parallel, a large number of researchers have also conducted work in validation methodology and validation experiments (*e.g*. Oberkampf, 2002, Roach, 1998).

In the present study, code verification will not be addressed, since the commercial code ANSYS CFX 12.0, used in this paper, has been verified independently by many authors in quite different contexts. ANSYS CFX has been successfully used in open-channel flow simulations (Babaeyan-Koopaei *et al*., 2003, Hõs and Kullmann, 2007, among others). Despite all these applications, there has been almost no attention given in compound channel flow studies to the issue of solution credibility. The work carried out here aims to evaluate the level of accuracy of CFD compared to experimental data obtained in a compound channel. For assessing the credibility of the application of commercial CFD code to compound channel flow (solution verification) where the correct solution is unknown, the authors have adopted the Grid Convergence Index (GCI). GCI values were computed using three different grid resolutions (fine, medium and coarse), after which a new mesh was established by refining locally the medium mesh in the regions where GCI results were higher. At the end of the refining process, a comparison of numerical results with the experimental data was performed.

2. THE GRID CONVERGENCE INDEX

The GCI was proposed by Roache in 1994, and it represents a simple method for reporting grid-convergence studies without any restriction to integer refinement (*e.g.* grid doubling). The GCI is based on generalized theory of Richardson extrapolation involving comparison of solutions at different grid spacing. In this study the procedure for estimation of GCI proposed by Journal of Fluid Engineering editorial policy was adopted (Celik, 2008).

For three-dimensional calculations, an average grid size h was calculated using

$$h = \left[\frac{1}{N} \sum_{i=1}^{N} \left(\Delta V_i \right) \right]^{1/3} \tag{1}$$

where ΔV_i is an average "global" volume of the cell, and N is the total number of cells of the calculation domain.

The simulations were run on three different grids (fine mesh 1, medium mesh 2, and coarse mesh 3) with the refinement factor between grids $r = h_{coarse} / h_{fine}$ > 1.1 (Roache, 1997). Since $h_1 < h_2 < h_3$ and $r_{21} = h_2/h_1$, $r_{32} = h_3/h_2$, where h_1, h_2 and h_3 are the grid sizes for fine, medium and coarse meshes accordingly, the calculation of the apparent order p of the algorithm can be performed using the expressions:

$$p = \frac{1}{\ln\left(r_{21}\right)} \left| \ln\left| \varepsilon_{32} / \varepsilon_{21} \right| + q\left(p\right) \right| \tag{2}$$

$$q\left(p\right) = \ln\left(\frac{r_{21}^{p} - s}{r_{32}^{p} - s} \right) \text{ and } s = 1 \cdot \operatorname{sign}\left(\varepsilon_{32} / \varepsilon_{21} \right) \tag{3}$$

where $\varepsilon_{32} = f_3 - f_2$, $\varepsilon_{21} = f_2 - f_1$, where f_1, f_2 and f_3 are the fine-, medium- and coarse-grid solution of the variable of interest obtained with grid spacing h_1, h_2 and h_3, respectively. For r = *constant*, $q(p) = 0$ and the order of accuracy p can be directly computed using Eq. (2).

Calculation of the extrapolated values:

$$f_{ext}^{21} = \left(r_{21}^{p} f_1 - f_2 \right) / \left(r_{21}^{p} - 1 \right) \text{ and } f_{ext}^{32} = \left(r_{32}^{p} f_2 - f_3 \right) / \left(r_{32}^{p} - 1 \right) \tag{4}$$

Approximate relative error:

$$e_a^{21} = \left| \frac{f_1 - f_2}{f_1} \right| \quad \text{and} \quad e_a^{32} = \left| \frac{f_2 - f_3}{f_2} \right| \tag{5}$$

Extrapolated relative error:

$$e_{ext}^{21} = \left| \frac{f_{ext}^{21} - f_1}{f_{ext}^{21}} \right| \quad \text{and} \quad e_{ext}^{32} = \left| \frac{f_{ext}^{32} - f_2}{f_{ext}^{32}} \right| \tag{6}$$

Roache (1997) defined the GCI for a particular grid as the error estimate multiplied by a factor of safety F_s:

$$GCI_{fine}^{21} = \frac{F_s e_a^{21}}{r_{21}^p - 1} \quad \text{and} \quad GCI_{fine}^{32} = \frac{F_s e_a^{32}}{r_{32}^p - 1} \tag{7}$$

where F_s = 1.25 has been adopted in this paper (*cf*. Roache, 1997).

3. NUMERICAL MODELLING

The flow field was calculated using the commercial 3D CFD code ANSYS CFX 12.0. The numerical scheme uses finite element-based control volume method, where the governing equations are discretized over each control volume. Advection terms in Navier-Stokes equations are discretized using second order high resolution scheme, shape functions are used to evaluate spatial derivatives for all the diffusion terms and pressure gradient terms. The resulting system is then solved in a coupled manner, and the results are interpolated to the grid nodes. In this paper, the flow dynamics is modeled by numerically solving Reynolds Averaged Navier-Stokes (RANS) equations for a water-air combination. To model the air-water segregated flow, the mass conservation of each phase is solved, while the momentum equation (RANS) for each phase is added up to eliminate the interface momentum transfer term. There is a closure equation for the volume fraction, which states that both phases volume fraction must add up to one at every fluid cell. The free surface model is accompanied by an interface sharpening algorithm, which guarantees a minimum diffusion of the volume fraction around the free surface. The stopping criterion for iterative calculations was set to be 0.001% for the normalized error in all equations, this led to an error of mass flow imbalance smaller then 0.1%.

The steady-state simulation was performed using the EARSM turbulence model. The EARSM represents an extension of the standard *k*-ε model which solves algebraic equations for Reynolds stresses; the model is derived from the Reynolds stress transport equations and gives a nonlinear relation between the Reynolds stresses and the mean strain-rate and vorticity tensors (Wallin & Johansson, 2000).

The domain, 0.785 m-wide and 10 m-long with a bed slope 0.001, is exactly coincident with the experimental flume; and was discretized using different meshes with hexahedral elements aligned to the main flow direction and refined for water region close to the walls, free surface and in the interface region between the main channel (MC) and the floodplain (FP) (Figure 1). For turbulence modeling near the channel bed, wall functions were used and the non-dimensional vertical coordinate, z^+, values of the element closest to the channel bed were kept around 30 for the FP and 50 for the MC. The bottom wall was prescribed with a non-slip boundary condition and an absolute roughness of 0.384 mm. The free surface is within the calculation domain, thus the flow includes both water and air.

A uniform velocity field with a water depth of 0.102 m and 5% of turbulence intensity was prescribed at the inlet; while a hydrostatic pressure profile with zero velocity derivatives was set at the outlet. The upper boundary condition was prescribed on the air, at 0.05 m above the expected free surface, with free-slip wall to allow the free motion of the air along the channel, facilitating the numerical robustness of the simulation.

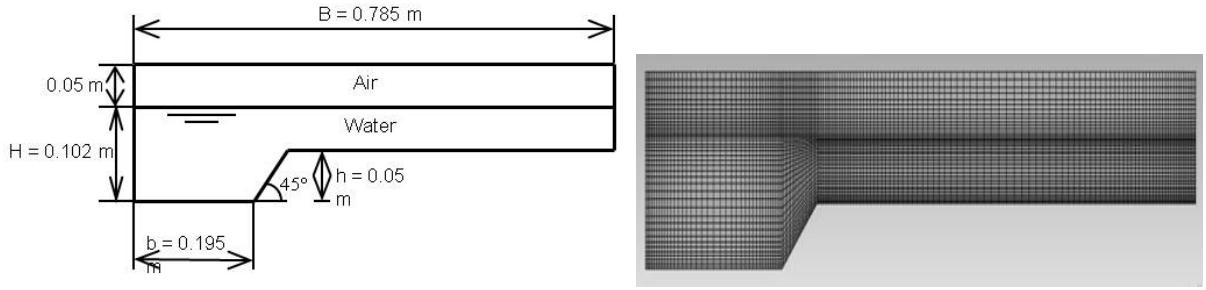

Figure 1 Cross-section of the compound channel domain and mesh 2.

4. RESULTS AND DISCUSSION

4.1. Solution Verification (GCI)

Determination of the GCI is based on the solutions of variables of interest (water time-averaged velocity components, TKE and dissipation) obtained with three different meshes. The establishment of those meshes will depend on the choice of the grid refinement factor, *r*. Although the most obvious choice would be *r* = 2, *i.e*. grid doubling (halving), this would lead to an increase of 2^3 of the number of volumes, resulting in an unaffordable computational time. Roache (1997) noted that it is neither necessary nor often desirable to use grid refinement factor *r* = 2, recommending a minimum 10% change in *r*. In this paper *r* = 1.2 was adopted in cross-section direction of the flow where the turbulence terms are more sensitive to the grid resolution. In streamwise direction the mesh was not refined since it is the least sensitive flow direction, thus the computational time of the simulation can be reduced without any direct effect on the credibility of the simulation (Hardy *et al*., 2003).

Since mesh doubling was not performed, an interpolation was necessary between mesh 1 and 3 and mesh 2 and 3 results to compare points of all grids. The apparent order of accuracy *p* was calculated directly using Eq. (2). The three meshes used in the GCI analysis are presented in the Table 1. The GCI was determined by considering cross-section at 7.5 m from the inlet (Figure 1), where the uniform flow has considered to be established.

Table 1 Meshes used in the GCI analysis. *Nx*, *Ny*, and *Nz* are the number of cells in the streamwise, spanwise and the vertical direction, respectively. N_{total} is the total number of cells

Mesh	N_x	N_y	N_z	N_{total}
1	200	192	48	1 843 200
2	200	152	44	1 337 600
3	200	148	36	1 065 600

Cross-section averaged GCI has been calculated only for the water region using the 3427 common data points in mesh 1, mesh 2 and mesh 3. The values of averaged GCI over a cross-section, at 7.5 m from the inlet, are given in Table 2 and presented on Figure 2.

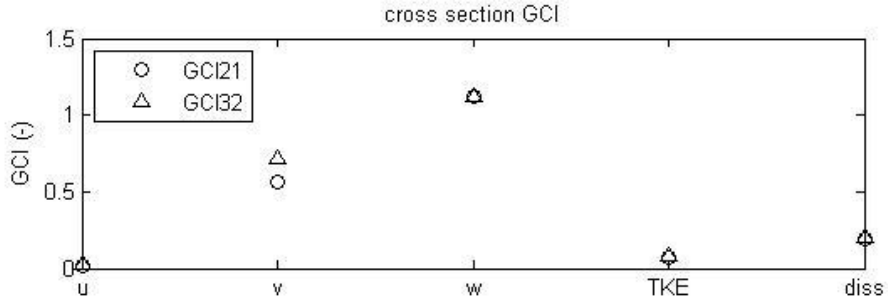

Figure 2 Cross-section averaged GCI for the velocity components, TKE and dissipation rate.

Table 2 Averaged GCI at cross-section 7.5 m downstream from inlet.

Variable of interest	*u*	*v*	*w*	TKE	Dissipation
GCI21 (%)	2.09	56.53	112.74	7. 40	19.20
GCI32 (%)	2.21	72.19	112.18	8.22	20.12

The lowest values of GCI, 2.09% and 2.21%, are for the streamwise velocity, *u*, the highest GCI values are for the spanwise and vertical velocities, *v* and *w*, respectively. This is not surprising because these components embody secondary flow and they are at least one order of magnitude smaller than *u* and therefore, are more sensitive to grid design. High GCI values for *v* and *w* demonstrate the mesh dependence of the secondary flow processes operating in the cross-section of the compound channel. The contours of GCI within the cross-section are presented in Figure 3.

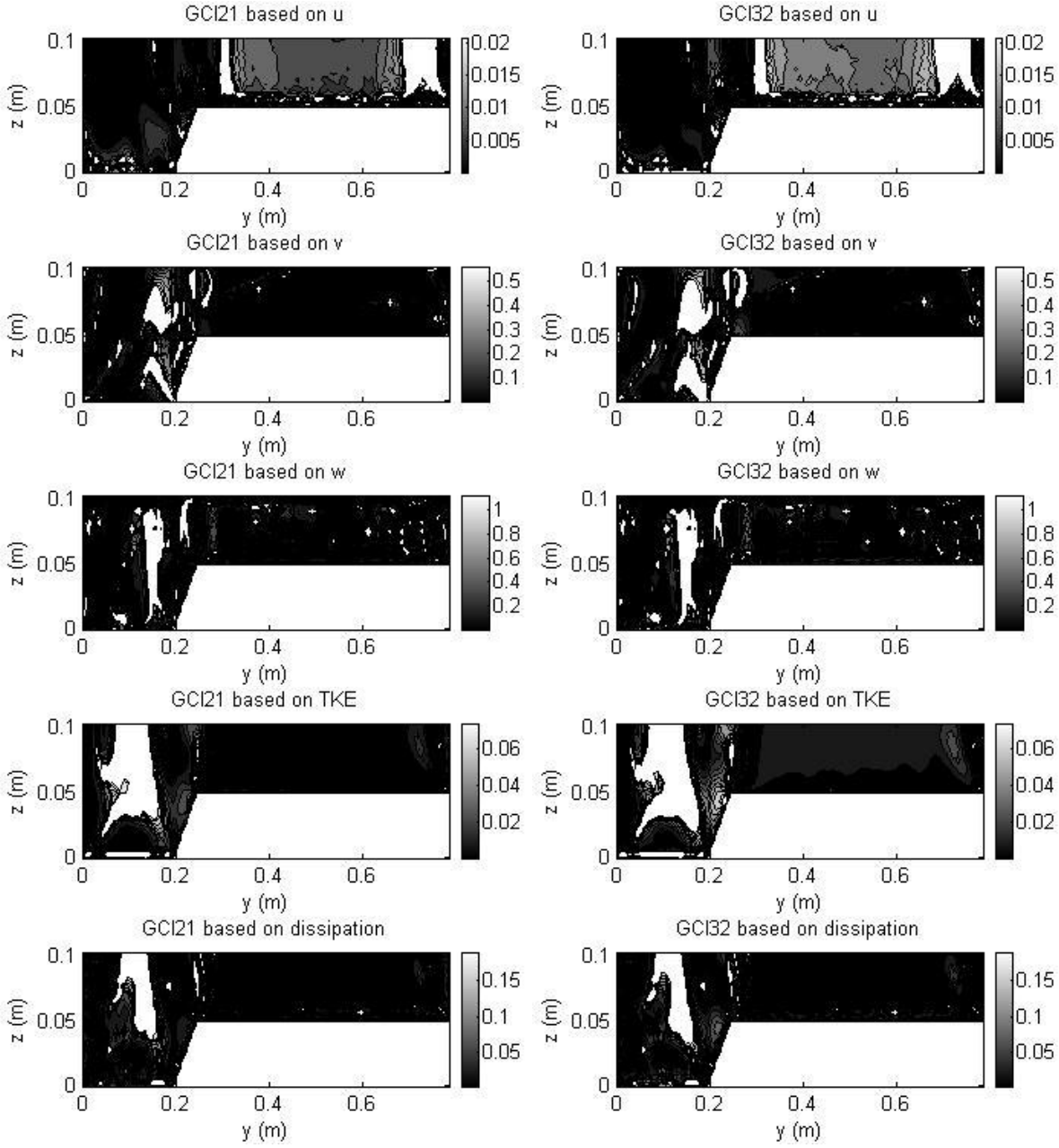

Figure 3 Contours of GCI for the three components of velocity, TKE and dissipation at cross-section 7.5 m downstream from inlet.

The upper limit of the scales in Figure 3 was limited to the average cross-section GCI21 for each variable. Therefore, the white spots on the plots represent regions where the GCI is higher than the

average. It is interesting to notice that the location of regions of higher GCI change according to the variable of interest, for *u* the worst results are in the floodplain, whereas for *v* and *w* they are located in the interface region and for TKE and the dissipation rate they are in the main channel. This would mean that to improve the GCI for all variables it would be necessary to refine the mesh in all the cross-section. However, looking at the GCI values of each variable it is clear that *v* and *w* present GCI values one order of magnitude higher than the other variables, meaning that secondary flow is more sensible to grid size than the computed turbulent field. Therefore, a higher spatial density is required to generate adequate system definition of secondary circulation.

Based on the GCI values of the spanwise and vertical velocities presented in Figure 5, mesh 2 was locally refined in the interface zone between the MC and the FP using a total of 1 584 000 hexahedron elements. Then the results were used to calculate new GCI21 and GCI32 values, using the same methodology mentioned above. After the refinement of mesh 2 the refinement factor became $r_{21} = 1.1$ and $r_{32} = 1.3$, thus the apparent order of accuracy was calculated applying Newton's iterative method to solve Eqs. (2) and (3).

The new values of GCI performed with refined mesh for cross-section 7.5 m from inlet are shown in the Figure 4 and in the Table 3. Comparing the cross-section averaged GCI presented in Figure 3 and Table 2 with the values obtained for the locally refined mesh (Figure 4 and Table 3), it is observed that the refinement allowed decreasing GCI values by one order of magnitude.

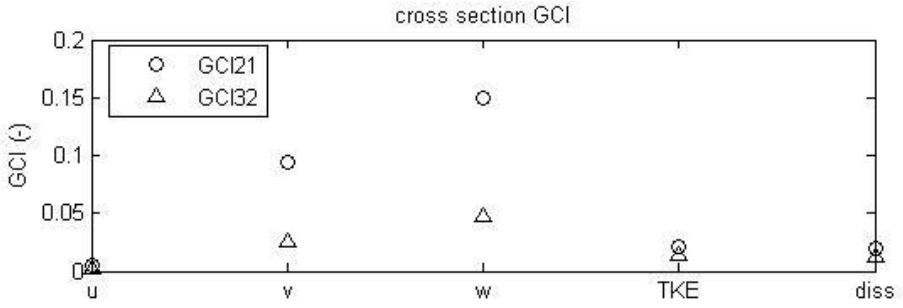

Figure 4 Cross-section averaged GCI for the velocity components, TKE and dissipation rate obtained with mesh 2 locally refined.

Table 3 Averaged GCI at cross-section 7.5 m from inlet obtained with mesh 2 locally refined.

Variable of interest	*u*	*v*	*w*	TKE	Dissipation
GCI21 (%)	0.50	9.44	14.98	2.13	2.02
GCI32 (%)	0.21	2.55	4.71	1.44	1.26

The contours of GCI for velocity components *v* and *w* within the cross-section are presented on Figure 5. The white zones (values above the average GCI) are smaller but more spread than for the not locally refined meshes (Figure 3), indicating that the number of nodes where GCI values are over the average value is smaller. But still there are some nodes where the GCI is very high, especially close to the wall where a special mesh resolution is required.

Analyzing the GCI results we can conclude that the numerical scheme has an acceptable numerical accuracy, especially for *u* since the cross-section averaged GCI is less than 1%. However, looking to other variables, like *v* and *w* components of velocity, the GCI values increase dramatically. This raises the issue of choosing the variable to which a scheme should be verified on. If the objective is only capturing the maximum longitudinal velocity, the scheme has converged and the numerical accuracy is acceptable. If the objective is to simulate mass transfer and secondary flow, the scheme is not capable yet to accurately predict lateral movement (*x-y* plan) and vertical movement (secondary flows in *y-z* plan); in this case, further mesh refinement is still necessary.

4.2. Validation (experimental data)

The experimental study was carried out in the Hydraulics Laboratory of the University of Beira Interior

in a 10 m long prismatic flume with bed slope S_0 = 0.1%, and asymmetric trapezoidal compound section (see Figure 1). The uniform regime was established by imposing a discharge of 23.0 l/s which corresponds to a relative height $h_r = (H - h)/H \approx 0.5$. The streamwise and vertical velocities of the flow were measured using a LDV. Positioning of the system probe was achieved with a 0.1 mm precision transversing system controlled by computer. The measurements were performed in back-scattering mode through the lateral glass of the channel. The water depth was measured using a point gauge; the total discharge was measured using an electromagnetic flow meter installed in the recirculation circuit of the flume.

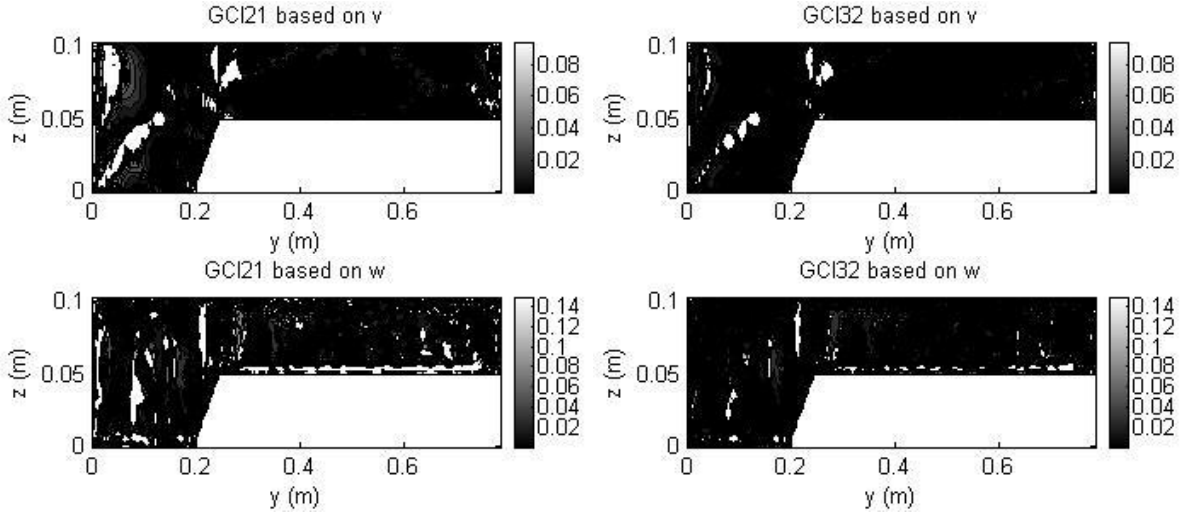

Figure 5 Contours of GCI for the *v* and *w* components of velocity at cross-section 7.5 m downstream from inlet obtained with mesh 2 locally refined.

Figure 6 presents the numerical results obtained with locally refined mesh 2 and the experimental results for *u* and *w* components of velocity for cross-section 7.5 m downstream from inlet. The experimental results presented here are only until *y* = 0.4 m, the maximum distance that LDV can measure. The numerical and experimental contours of *u* component of velocity show similar behavior: the isovels bulge significantly upward near the upper interface as a result of secondary flow cells generated by turbulence anisotropy. The main difference between numerical results and experimental data is that the numerical model cannot capture the effect of free surface, where the maximum velocities occur below the free surface (Nezu, 1994).

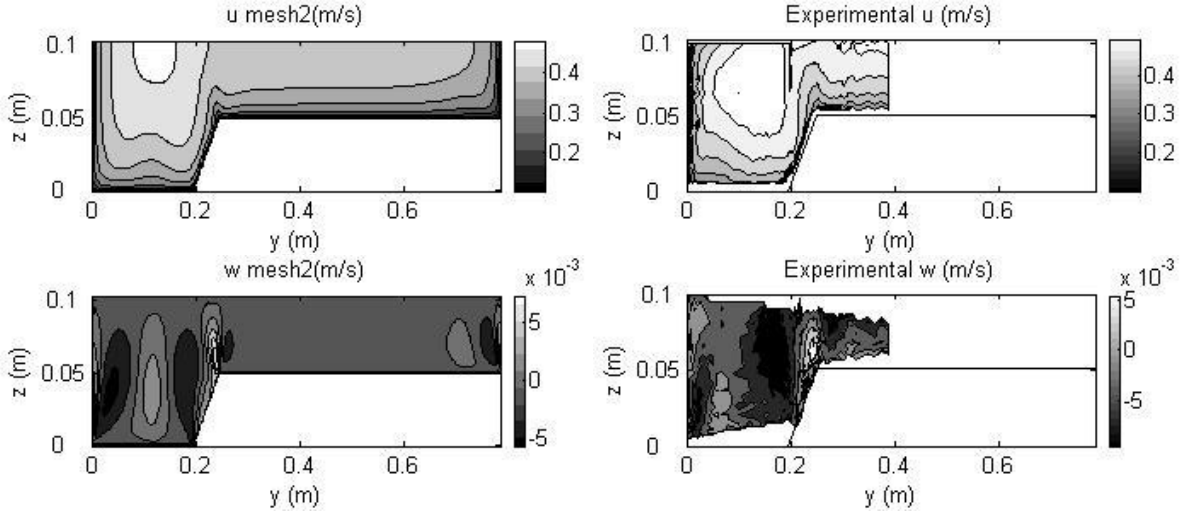

Figure 6 Comparison of *u*- and *w*- components of velocity obtained numerically (left) using EARSM and experimentally (right) using LDV at cross-section 7.5 m downstream from inlet of the compound channel.

The numerical and experimental contours of *w* component of velocity show similar pattern, *i.e*. the positive and negative velocities are in the same locations. Two secondary flow cells interact near the upper interface and are responsible for pushing upwards particles with smaller velocities, causing the inflection of *u* isovel lines. In the main channel, near the lower interface, it can also be observed the interaction of two secondary cells that direct the flow downwards and therefore inflect the isovel lines in that direction. The two secondary flow cells exiting in the main channel interact in the middle of the main channel directing the flow upwards, but with less intensity than what is observed in the upper interface. Near the wall, the secondary cell points downward, causing an effect similar to what has been referred for the lower interface. The numerical and experimental values of *w* are in the same range. However, for the experimental results the downward values are higher and the upward values are smaller than the numerical ones.

5. CONCLUSION

A GCI method for solution verification of a 3D CFD scheme for compound channel was applied. The results show that, despite the solution for the streamwise velocity can be considered acceptable, the other velocity components still presented high GCI values requiring further mesh refinement. This conclusion is important, since in the majority of CFD studies solution verification is done only using the streamwise velocity and researchers rely on this convergence criterion to infer physical limitations of the model in predicting some secondary patterns of the flow. If the other velocity components still have high GCI values, the secondary flow field is still mesh dependent and further refinement is needed prior to taking any conclusions about model limitations. The validation has shown good agreement between numerical and experimental results; the maximum velocities and the interaction zones of secondary flow cells were predicted, although some small discrepancies are found in the magnitude of the values.

6. ACKNOWLEDGMENTS

The authors wish to acknowledge the financial support of the Portuguese Foundation for Science and Technology through the project PTDC/ECM/70652/2006. The first and second authors wish to acknowledge the financial support of the Portuguese Foundation for Science and Technology through the Grants No. SFRH/BD/64337/2009 and SFRH/BD/33646/2009, respectively.

7. REFERENCES

1. Babaeyan-Koopaei K., Ervine D.A. and Pender G. (2003), *Field Measurements and Flow Modeling of Overbank Flows in River Severn, U.K*., Journal of Environmental Informatics, 1 (1), 28-36.
2. Celik, I. (2008), *Procedure for Estimation and Reporting of Uncertainty Due to Discretization in CFD Applications*, ASME J. Fluids Eng, 130.
3. Hardy R.J., Lane S.N., Ferguson R.I. and Parsons D.R. (2003), *Assessing the credibility of a series of computational fluid dynamic simulations of open channel flow*, Hydrological Processes, 17, 1539-1560.
4. Hõs,C. and Kullmann, L. (2007), *A numerical study on the free-surface channel flow over a bottom obstacle,* Journal of Computational and Applied Mechanics, 8 (1), 57-70.
5. Nezu, I. (1994), *Compound Open-Channel Turbulence and its Role in River Environment*, Keynote address, APD-IAHR Congress, Singapore, August 24.
6. Oberkampf W.L., Trucano T.G. (2002), *Verification and Validation in Computational Fluid Dynamics*, Sandia National Laboratories, SAND2002-0529, Albuquerque, NM, 2002.
7. Roache, P.J. (1997), *Quantification of Uncertainty in Computational Fluid Dynamics*, Annual Review of Fluid Mechanics, 29, 123-160.
8. Roache, P.J. (1998), *Verification and Validation in Computational Science and Engineering*, Hermosa Publishers, Albuquerque, NM.
9. Wallin, S. and Johansson, A. (2000), *An explicit algebraic Reynolds stress model for incompressible and compressible turbulent flows*, Journal of Fluid Mechanics, 403, 89-132.